Received: 1 August 2022 | Revised: 24 May 2023 | Accepted: 22 July 2023

IET Microwaves, Antennas & Propagation

DOI: 10.1049/mia2.12399

ORIGINAL RESEARCH

Miniaturised integrated passive device balun design with balanced amplitude and phase for Wi-Fi applications

Qixiang Ren | **Yazi Cao** | **Bo Yuan** | **Yanzhu Qi** | **Shichang Chen** | **Gaofeng Wang**

School of Electronics and Information, Hangzhou Dianzi University, Hangzhou, China

Correspondence

Yazi Cao and Bo Yuan, School of Electronics and Information, Hangzhou Dianzi University, Hangzhou, China.
Email: yazi.cao@hotmail.com and yuanbo@hdu.edu.cn

Funding information

National Natural Science Foundation of China, Grant/Award Numbers: 61971171, 62141409; National Key Research and Development Program of China, Grant/Award Number: 2019YFB2205003

Abstract

A miniaturised integrated passive device (IPD) balun design with low insertion loss and balanced amplitude and phase is proposed for Wi-Fi/Bluetooth applications. In this design, a novel topology based on the modified T-type filter structure is introduced to offset the parasitic and coupling effects that cause poor balance in IPD design. The proposed balun design is fabricated on a GaAs substrate. The measured insertion loss is lower than 0.9 dB and the measured return loss is >16 dB in the frequency range of 2.2–2.9 GHz. The measured results of amplitude and phase show rather minor imbalances, which are lower than ±0.67 dB and ±1.8° respectively. The fabricated device size is 0.9 mm × 0.6 mm only.

KEYWORDS

baluns, filters

1 | INTRODUCTION

With the rapid development of mobile communications, it makes a strong requirement for electronic devices to be compact, lightweight, multi-functional, and high performance. As a result, the system in package (SIP) technology, as an important technical route beyond Moore's Law at the integrated packaging level, has received more and more attention and applications. An integrated passive device (IPD) has recently been widely used and became an important puzzle for implementing SIP. In the literature, IPD has been used to realise microwave components like bandpass filters [1, 2], power dividers [3, 4], baluns [5–13] and etc.

Baluns are the key passive devices in balanced microwave front-end circuits such as balanced mixers, antenna feed networks and push-pull amplifier [6, 14, 15]. Baluns convert signal from unbalance to balance with half of the input signal amplitude and the phase delay difference of 180° at two out terminals. Usually, passive baluns are classified by lumped-element baluns [5–7], Marchand baluns [8, 9], and transformer baluns [10, 11, 13]. The widely used distributed structure is more suitable for high frequency band (>4 GHz), such as Marchand baluns. However, at low frequencies distributed structure consumes too much of the expensive chip area and are therefore not suitable for MMICs. In this case, lumped-element baluns exampled by a second-order lattice type composed of T-junction low/high-pass filters were candidates for IPD circuit [5–7]. But for chip-level design, the parasitic effects of lumped circuit devices and the coupling effects between them had an influence on the performance. Chen et al. [5] addressed on the theory of second-order lattice type balun by ABCD matrix arrangement results for inductor and capacitor's value calculated accurately. Kumar et al. [7] used the traditional T-filter structure balun as an example, the results of the parasitic effect calculation are discussed.

In this letter, a miniaturised GaAs-based IPD balun design with low insertion loss and balanced amplitude and phase is proposed. In this design, a novel topology based on the modified T-type filter structure is introduced to offset the parasitic and coupling effects that cause poor balance. In the following sections, the proposed balun design using the modified T-junction network is analysed. The simulation results from the

electromagnetic (EM) simulator UltraEM [16] as well as the measured results are included to illustrate and validate the effectiveness of the proposed design.

2 | DESIGN ANALYSIS

Traditional lumped-element balun design is built upon a T-junction topology integrating the T-type low/high-pass filter concept [5–7]. By combining the phase lag and advance characteristics of low-pass filter (LPF) and high-pass filter (HPF) respectively, a phase difference of 180° between two outputs can be achieved.

But in the IPD design, the in-band phase and amplitude balance of the traditional circuit is not good in layout simulation. In general, the inductors can greatly affect the actual balun layout structure since the inductors occupy most of the IPD layout area. A parallel inductor L_4 is herein introduced at the output of the HPF. A suitable parallel inductance can improve the amplitude and phase balance within the operation frequency.

To analyse the modified T-type filter structure, the low/high-pass filters can be treated as lossless transmission lines with phase delay of ±90° respectively. Unfortunately, the modified T-junction network makes the absence of symmetry on the circuit. Hence, two frequency transformation factors and two impedance transformation factors are introduced to low/high-pass filter respectively. The proposed balun structure with the modified T-junction network is illustrated in Figure 1.

The ABCD matrix of a lossless transmission line can be written as

$$\begin{bmatrix} A & B \\ C & D \end{bmatrix} = \begin{bmatrix} \cos\gamma & jZ_0\sin\gamma \\ jY_0\sin\gamma & \cos\gamma \end{bmatrix} \tag{1}$$

where Z_0 is the characteristic impedance, Y_0 is the characteristic admittance, and γ is the phase shift of the lossless transmission line.

One the other hand, the ABCD matrix can be applied to the individual arm of the proposed balun circuit in Figure 1. The ABCD matrix of the LPF consisting of two series inductors and a shunt capacitor can be expressed as

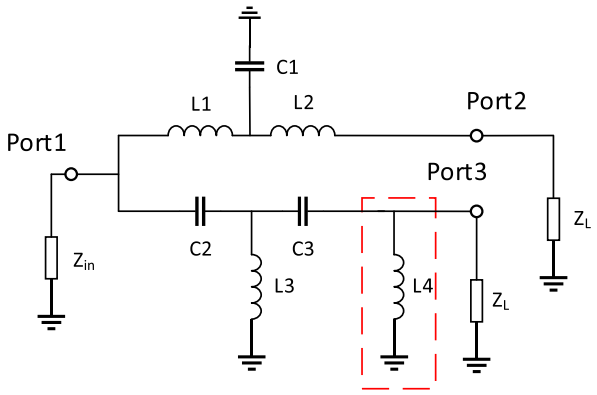

FIGURE 1 Schematic of the proposed balun with a parallel inductor L4.

$$\begin{aligned} \begin{bmatrix} A & B \\ C & D \end{bmatrix}_{\mathrm{LPF}} &= \begin{bmatrix} 1 & jX_{\mathrm{L1}} \\ 0 & 1 \end{bmatrix}\begin{bmatrix} 1 & 0 \\ jB_{\mathrm{C1}} & 1 \end{bmatrix}\begin{bmatrix} 1 & jX_{\mathrm{L2}} \\ 0 & 1 \end{bmatrix} \\ &= \begin{bmatrix} 1-X_{\mathrm{L1}}B_{\mathrm{C1}} & jX_{\mathrm{L2}}(1-X_{\mathrm{L1}}B_{\mathrm{C1}})+jX_{\mathrm{L1}} \\ jB_{\mathrm{C1}} & 1-X_{\mathrm{L2}}B_{\mathrm{C1}} \end{bmatrix} \end{aligned} \tag{2}$$

By making the ABCD matrix of lossless transmission line ($\gamma = 90°$) equal to that of the low-pass prototype, one obtains

$$\begin{aligned} &\begin{bmatrix} \cos\gamma & jZ_0\sin\gamma \\ jY_0\sin\gamma & \cos\gamma \end{bmatrix} \\ &= \begin{bmatrix} 1-X_{\mathrm{L1}}B_{\mathrm{C1}} & \mathrm{j}X_{\mathrm{L2}}(1-X_{\mathrm{L1}}B_{\mathrm{C1}})+jX_{\mathrm{L1}} \\ jB_{\mathrm{C1}} & 1-X_{\mathrm{L2}}B_{\mathrm{C1}} \end{bmatrix} \end{aligned} \tag{3}$$

where $X_{Li} = \omega_{\mathrm{LPF}}L_i$, $B_{Ci} = \omega_{\mathrm{LPF}}C_i$ ($i = 1, 2$), $\omega_{\mathrm{LPF}} = n_1 \cdot \omega$ (ω is centre frequency), and $Z_{01} = m_1 \cdot \sqrt{Z_{in} \cdot 2Z_L}$. The values of L_1, L_2, and C_1 are given as

$$\begin{cases} L_1 = L_2 = \dfrac{Z_{01}}{\omega_{\mathrm{LPF}}} = \dfrac{m_1 \cdot \sqrt{Z_{\mathrm{in}} \cdot 2Z_L}}{n_1 \cdot \omega_0} \\ C_1 = \dfrac{1}{\omega_{\mathrm{LPF}} \cdot Z_{01}} = \dfrac{1}{n_1 \cdot \omega_0 \cdot \sqrt{Z_{\mathrm{in}} \cdot 2Z_L}} \end{cases} \tag{4}$$

Similarly, the ABCD matrix of the HPF consisting of two series capacitors and two shunt inductors can be given as

$$\begin{aligned} \begin{bmatrix} A & B \\ C & D \end{bmatrix}_{\mathrm{HPF}} &= \begin{bmatrix} 1 & -jX_{\mathrm{C2}} \\ 0 & 1 \end{bmatrix}\begin{bmatrix} 1 & 0 \\ -jB_{\mathrm{L3}} & 1 \end{bmatrix}\begin{bmatrix} 1 & -jX_{\mathrm{C3}} \\ 0 & 1 \end{bmatrix}\begin{bmatrix} 1 & 0 \\ -jB_{\mathrm{L4}} & 1 \end{bmatrix} \\ &= \begin{bmatrix} (1-X_{\mathrm{C2}}B_{\mathrm{L3}})(1-X_{\mathrm{C3}}B_{\mathrm{L4}})-X_{\mathrm{C2}}B_{\mathrm{L4}} & -jX_{\mathrm{C3}}(1-X_{\mathrm{C2}}B_{\mathrm{L3}})-jX_{\mathrm{C2}} \\ -jB_{\mathrm{L4}}(1-X_{\mathrm{C3}}B_{\mathrm{L3}})-jB_{\mathrm{L4}} & 1-X_{\mathrm{C3}}B_{\mathrm{L3}} \end{bmatrix} \end{aligned} \tag{5}$$

By making the ABCD matrix of lossless transmission line ($\gamma = -90°$) equal to that of the HPF, one obtains

$$\begin{bmatrix} \cos\gamma & jZ_0\sin\gamma \\ jY_0\sin\gamma & \cos\gamma \end{bmatrix} = \begin{bmatrix} (1-X_{C2}B_{L3})(1-X_{C3}B_{L4})-X_{C2}B_{L4} & -jX_{C3}(1-X_{C2}B_{L3})-jX_{C2} \\ -jB_{L4}(1-X_{C3}B_{L3})-jB_{L3} & 1-X_{C3}B_{L3} \end{bmatrix} \tag{6}$$

where $B_{Li} = 1/\omega_{HPF}L_i$, $X_{Ci} = 1/\omega_{HPF}C_i$ ($i = 2, 3, 4$), $\omega_{HPF} = \omega_0/n_2$ and $Z_{02} = m_2 \cdot \sqrt{Z_{in} \cdot 2Z_L}$. The values of L_3, L_4, C_2, and C_3 can be calculated as

$$\begin{cases} C_3 = \dfrac{1}{\omega_{HPF}Z_{02}} = \dfrac{n_2}{\omega_0 \cdot m_2 \cdot \sqrt{Z_{in} \cdot 2Z_L}} \\ L_3 = \dfrac{Z_{02}}{\omega_{HPF}} = \dfrac{n_2 \cdot m_2 \cdot \sqrt{Z_{in} \cdot 2Z_L}}{\omega_0} \\ L_4 = \dfrac{{Z_{02}}^2 \cdot C_2}{\omega_{HPF} \cdot Z_{02} \cdot C_2 - 1} = \dfrac{n_2 \cdot {m_2}^2 \cdot Z_{in} \cdot 2Z_L \cdot C_2}{\omega_0 \cdot m_2 \cdot \sqrt{Z_{in} \cdot 2Z_L} \cdot C_2 - n_2} \end{cases} \tag{7}$$

Figure 2a–h show the optimisation results of the phase and amplitude imbalance affected by four transformation factors. Assume that the design specifications are herein set as $Z_{in} = Z_L = 50\ \Omega$, $f_0 = 2.45$ GHz, $n_1 = 1.064$, $m_1 = 0.903$, $n_2 = 0.94$, $m_2 = 0.896$. The theoretical inductors and capacitors can be then evaluated from Equations (4) and (7), that is, $C_1 = 0.96$ pF, $C_2 = 5.22$ pF, $C_3 = 0.96$ pF, $L_1 = L_2 = 3.9$ nH, $L_3 = 3.87$ nH, and $L_4 = 4.75$ nH.

3 | PROTOTYPE AND EXPERIMENTAL RESULTS

3.1 | Fabrication process

The proposed IPD balun design is implemented by using the thin-film process technology on a GaAs substrate. The cross section is illustrated in Figure 3. The GaAs substrate has thickness of 100 μm. On top of the substrate, it provides two metal layers (M1 and M2) and six dielectric layers composed of three kinds of dielectric (Si_3N_4, SiCN, and BCB). This thin-film technology allows a high level of integration and realisation of passive elements, such as inductors, capacitors, and resistors.

3.2 | Simulated and measured results

In Figure 4, a set of EM simulated results are depicted to illustrate the effects of the proposed parallel inductor L_4. As can be seen, L_4 can improve the amplitude and phase balance at the two output terminals. Therefore, it can be well adjusted to correct the bad balance of the original circuit in the layout by adjusting the value of L_4. The detail dimensions of spiral inductor and MIM capacitor in Figure 1 are listed in Table 1.

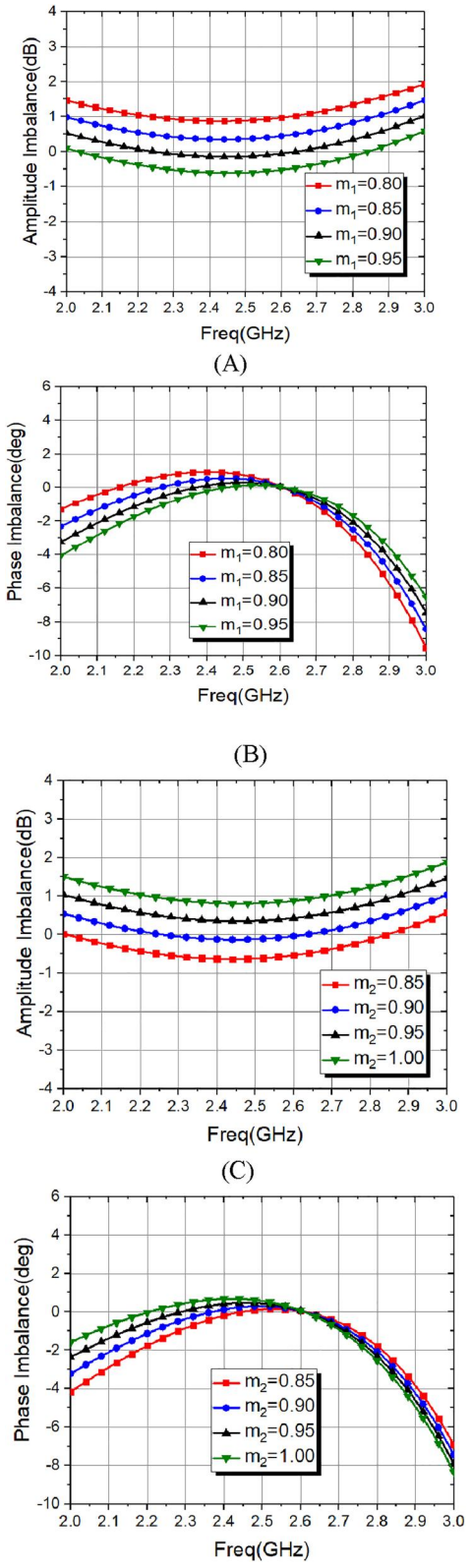

FIGURE 2 (a–h) The optimisation results of the phase and amplitude imbalance affected by four transformation factors.

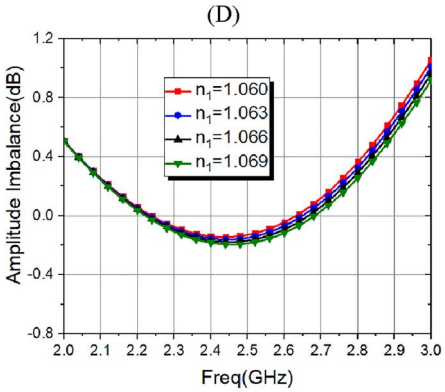

FIGURE 2 (Continued)

Based on the above-mentioned analysis, the proposed balun is simulated and its GDS layout is generated by EM simulator UltraEM from Faraday Dynamics, Inc. [16]. Figure 5 shows the chip layout and the micrograph of the proposed GaAs-based balun design. The 3-port balun is evaluated by using the following equations:

$$\mathrm{IL} = -10\log_{10}\left(|S_{21}|^2 + |S_{31}|^2\right) \tag{8}$$

$$\text{Amplitude Imbalance} = 20 \cdot \log_{10}|S_{21}/S_{31}| \tag{9}$$

$$\text{Phase Imbalance} = 180^\circ \pm \left|\tan^{-1}\frac{\mathrm{Im}(S_{21}/S_{31})}{\mathrm{Re}(S_{21}/S_{31})}\right| \tag{10}$$

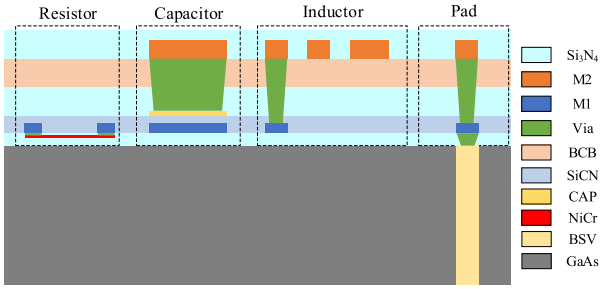

FIGURE 3 Cross-sectional view of the GaAs-based integrated passive device.

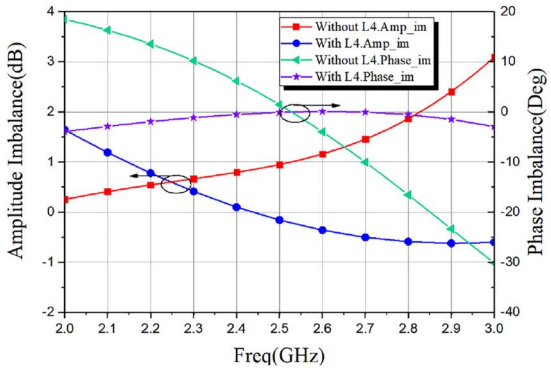

FIGURE 4 Amplitude imbalance and phase imbalance with/without L_4.

TABLE 1 Fabricated dimensions of elements in the proposed balun.

Inductor	L_1	L_2	L_3	L_4
Inner diameter (μm)	110.39	108.99	27.2	47.99
Width (μm)	8.27	9.37	6.25	7.44
Space (μm)	4	4	4	4
Number of turns	4.5	4.5	7.5	6.25
Q-factor	18.87	19.72	12.51	11.51
Capacitor	C_1	C_2		C_3
Width (μm)	42.25	65.62		20.38
Length (μm)	21.94	73.35		57.67
Q-factor	421.91	105.26		35.34

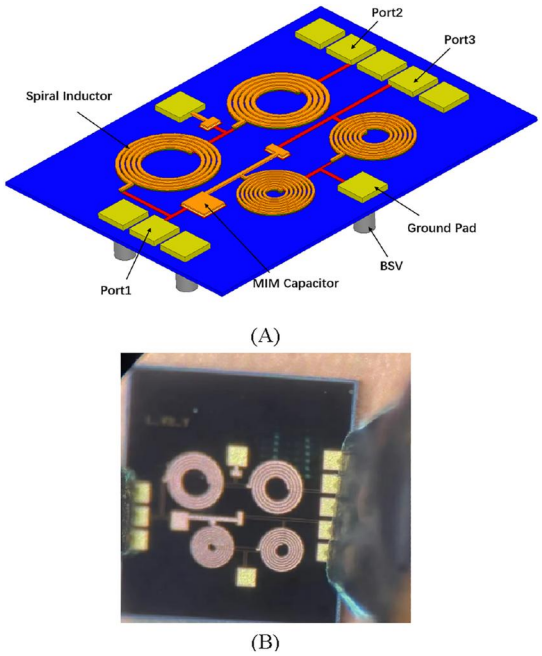

FIGURE 5 (a) Chip layout view and (b) Micrograph of the proposed balun.

The fabricated balun is measured on-chip using the Keysight N5244A PNA-X vector network analyser and Cascade summit-11000 probe station. The simulated and measurement results of the proposed balun are compared in Figure 6. It is clear that the simulation results are in good agreement with the measured ones. At the operating frequency band (2.2–2.9 GHz), it achieves an insertion loss lower than 0.9 dB and a return loss better than 16 dB, as shown in Figure 6a. There exists some minor frequency shift between the simulated and measured results. This is mainly attributed to the fabricated tolerance and model inaccuracy. Figure 5b illustrates the measured amplitude and phase imbalance, in which the imbalances within ±0.67 dB and ±1.8° from 2.2 to 2.9 GHz have been obtained respectively.

Comparing to the previous designs as shown in Table 2, the proposed balun design has the improved imbalance responses which can be attributed to the modified T-type filter structure. In addition, the proposed balun design achieve miniaturisation due to compact on-chip spiral inductor by using the thin-film process technology on a GaAs substrate.

4 | CONCLUSION

In this letter, a miniaturised balun design with low insertion loss and balanced amplitude and phase has been presented. One parallel inductor was introduced to offset the parasitic and coupling effects that cause poor balance in the proposed balun design. The proposed balun design was fabricated on a GaAs substrate. The measured results are in good agreement with the simulated results. The fabricated balun device has a size of 0.9 × 0.6 mm, which is used in various RF SIP modules for Wi-Fi mobile applications.

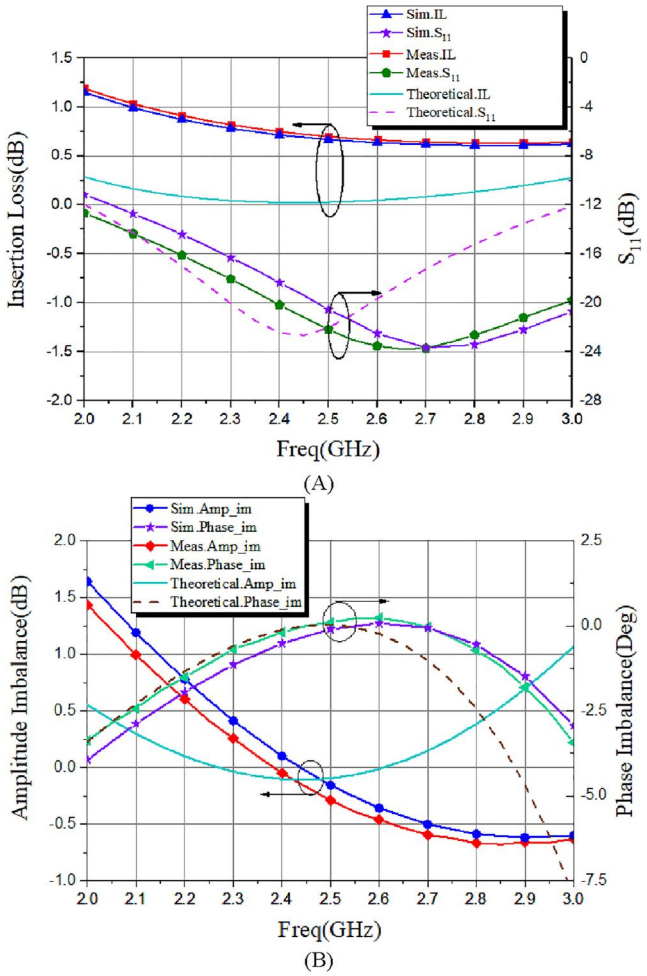

FIGURE 6 Simulated and measured results of the proposed balun: (a) S_{11} and insertion loss; (b) amplitude and phase imbalance.

TABLE 2 Comparison of the proposed balun with several reported integrated passive device LC-baluns.

Ref.	[5]	[6]	[7]	[13]	This work
Substrate technology	Silicon	GaAs	GaAs	Silicon	GaAs
Frequency band (GHz)	1.5–2.1	2.4–2.5	0.5–5	4.9–5.9	2.2–2.9
Amplitude imbalance (dB)	0.2	1	0.47 (min)	1.07	0.67
Phase imbalance (degrees)	2	3	3	2.6	1.8
Effective area (mm^2)	1.65 × 1.5	0.8 × 0.7	1.7 × 0.8	0.93 × 1.24	0.9 × 0.6

Abbreviation: LC, lumped circuit.

AUTHOR CONTRIBUTIONS

Qixiang Ren: Writing – original draft; writing – review & editing. **Yazi Cao**: Formal analysis; supervision; writing –

original draft; writing – review & editing. **Bo Yuan**: Supervision; writing – review & editing. **Yanzhu Qi**: Writing – original draft; writing – review & editing. **Shichang Chen**: Writing – original draft; writing – review & editing. **Gaofeng Wang**: Writing – original draft; writing – review & editing.

ACKNOWLEDGEMENTS

The paper was funded by the National Natural Science Foundation of China under Grant 62141409, Grant 61971171, the National Key Research and Development Program of China under Grant 2019YFB2205003 and the Zhejiang Provincial Key Research & Development Project under Grant 2021C01041.

CONFLICT OF INTEREST STATEMENT

The authors declare no potential conflict of interests.

DATA AVAILABILITY STATEMENT

The datasets generated or analysed during this study are available from the corresponding author on reasonable request.

ORCID

Yazi Cao https://orcid.org/0000-0001-6636-3662
Shichang Chen https://orcid.org/0000-0003-1628-5429

REFERENCES

1. Shen, G., et al.: Millimeter-wave dual-band bandpass filter with large bandwidth ratio using GaAs-based integrated passive device technology. IEEE Electron. Device Lett. 42(4), 493–496 (2021). https://doi.org/10.1109/led.2021.3062862
2. Lyu, Y.-P., et al.: Compact and high-order on-chip wideband bandpass filters on multimode resonator in integrated passive device technology. IEEE Electron. Device Lett. 43(2), 196–199 (2022). https://doi.org/10.1109/led.2021.3139623
3. Cheng, J.-D., et al.: An unequal Wilkinson power divider based on integrated passive device technology and parametric model. IEEE Microw. Wireless Compon. Lett. 32(4), 281–284 (2022). https://doi.org/10.1109/lmwc.2021.3126850
4. Hsiao, C.-Y., Wu, C.-T.M., Kuo, C.-N.: A W-band 1-dB insertion loss Wilkinson power divider using silicon-based integrated passive device. IEEE Microw. Wireless Compon. Lett. 31(6), 654–657 (2021). https://doi.org/10.1109/lmwc.2021.3066344
5. Chen, K., Fang, B., Yeh, H.: IPD broadband balun design for GSM applications. In: 2010 IEEE Electrical Design of Advanced Package & Systems Symposium, pp. 1–4 (2010)
6. Wang, C., Kim, N.Y.: High performance WLAN balun using integrated passive technology on SI-GaAs substrate. Microw. Opt. Technol. Lett. 54(5), 1301–1305 (2012). https://doi.org/10.1002/mop.26801
7. Kumar, A., et al.: Design analysis of integrated passive device-based balun devices with high selectivity for mobile application. IEEE Access 7, 23169–23176 (2019). https://doi.org/10.1109/access.2019.2898513
8. Chin, H.-W., et al.: Design of an IPD ultra wideband Marchand balun using a phase compensation line. In: 2015 Asia-Pacific Microwave Conference (APMC) (2015)
9. Li, Y., et al.: A 1.34-to-16.37-GHz on-chip balun based on asymmetric stacked spiral transformers. Electron. Lett. 56(8), 121–123 (2019). https://doi.org/10.1049/el.2019.3428
10. Aliqab, K., Hong, J.: Fully embedded ultra-wideband multilayer balun into organic packaging substrate. IET Microw. Antennas Propag. 13(3), 322–325 (2019). https://doi.org/10.1049/iet-map.2018.5859
11. Choi, H.-W., et al.: 1-W, high-gain, high-efficiency, and compact sub-GHz linear power amplifier employing a 1:1 transformer balun in 180-nm CMOS. IEEE Microw. Wireless Compon. Lett. 30(8), 779–781 (2020). https://doi.org/10.1109/lmwc.2020.3002234
12. Wong, K.W., Mansour, R.R., Weale, G.: Reconfigurable bandstop and bandpass filters with wideband balun using IPD technology for frequency agile applications. IEEE Trans. Compon. Packag. Manuf. Technol. 7(4), 610–620 (2017). https://doi.org/10.1109/tcpmt.2017.2667580
13. Chung, H., et al.: Design of step-down broadband and low-loss Ruthroff-type baluns using IPD technology. IEEE Trans. Compon. Packag. Manuf. Technol. 4(6), 967–974 (2014). https://doi.org/10.1109/tcpmt.2014.2311662
14. Lin, S.W., Chiu, H.C., Fu, J.S.: High-efficiency Ka band microwave monolithic integrated circuit frequency tripler using lumped-element balun. IET Microw. Antennas Propag. 5(1), 30 (2011). https://doi.org/10.1049/iet-map.2009.0514
15. Zhong, C., et al.: Miniaturized wideband four-way out-of-phase power divider based on Marchand balun. IET Microw. Antennas Propag. 13(15), 2682–2686 (2019). https://doi.org/10.1049/iet-map.2019.0465
16. UltraEM V202109. Faraday Dynamics, Inc., Hangzhou (2022)

How to cite this article: Ren, Q., et al.: Miniaturised integrated passive device balun design with balanced amplitude and phase for Wi-Fi applications. IET Microw. Antennas Propag. 18(1), 1–6 (2024). https://doi.org/10.1049/mia2.12399